Proceedings of ASME Turbo Expo 2013: Turbine Technical Conference and Exposition
GT2013
June 3-7, 2013, San Antonio, Texas, USA

GT2013-95423

MULTI-OBJECTIVE OPTIMIZATION OF A U-BEND FOR MINIMAL PRESSURE LOSS AND MAXIMAL HEAT TRANSFER PERFORMANCE IN INTERNAL COOLING CHANNELS

Tom Verstraete, Jing Li

von Karman Institute for Fluid Dynamics
Turbomachinery and Propulsion Department
Chaussée de Waterloo 72
1640 Rhode-Saint-Genèse, Belgium
Email: tom.verstraete@vki.ac.be, jing4@kth.se

ABSTRACT

A multi-objective design optimization is performed on a U-bend in serpentine internal cooling channels. The aim is to achieve both minimized total pressure loss and maximized heat transfer ability. The optimization technique used is a two-level routine developed at the Von Karman Institute for Fluid Dynamics (VKI), featuring a Differential Evolution algorithm assisted by a metamodel, which is continuously updated during the course of the optimization process to increase its accuracy. The geometries are carefully parameterized by means of Bezier curves. In total, 26 geometrical parameters are used as design variables, allowing an extensive variation of the U-bend geometries. The fluid dynamic and heat transfer performances of the selected geometries are predicted by a Reynolds-averaged Navier-Stokes solver in OpenFOAM. The result shows that dozens of optimized geometries of enhanced performances in both design objectives can be obtained after a few numbers of iterations. The enhancement ranges from roughly 12~30% decrease in total pressure loss and a 8~17% increase in heat flow rate. A clear trade-off between pressure loss and heat transfer is observed, allowing designers to select a compromising geometry between both criteria after the optimization process, depending on the application type of the internal cooling channel. Generally, a stronger secondary flow motion in the channel will be responsible for higher heat transfer at the cost of increased losses. A discussion is held on the geometrical features that have an impact on the secondary flow motion strength and lead to general applicable conclusions.

INTRODUCTION

The thermal efficiency of gas turbines increases dramatically with the maximum temperature of the cycle. As a result, state-of-the-art gas turbines are designed to operate at turbine inlet temperatures that approach 2000 K. Since the materials commonly employed for the turbine components cannot withstand temperatures above 1350 K, effective cooling must be applied along the hot-gas-path in order to guarantee safe functioning. In most cases the coolant is air bled from the high pressure compressor, which bypasses the combustor and enters the blade through its root, circulating through serpentine internal passages. The flow in internal cooling channels is fully turbulent and generally free of compressibility effects. The geometrical configurations are complex and the velocity field is highly three-dimensional. More than 20% of the discharge air from the compressor is used to cool the high pressure turbine, leading to a severe penalty on the thermodynamic efficiency. Therefore, an effective design must be able to maintain the metal temperature below acceptable limits with minimal coolant mass flow rates and pressure drop penalties. Reviews of mechanisms and performances of turbine blade cooling techniques were presented, among others, by Han et al. [1] and Weigand et al. [2].

Among the salient features of the cooling passages, the U-bends that connect consecutive passages play a key role, as they represent regions of strong pressure loss, especially for small radius ratio (mean bend radius/duct hydraulic diameter): in this case the bend region can be responsible for up to 25% of the pressure loss in the entire multi-pass cooling system. Consequently this flow configuration has received profound attention from the scientific and technical community.

Numerous experiments investigating the turbulent flow in 180° bends have been conducted, both for circular and sharp turns. The contributions of Humphrey et al. [3], Chang et al. [4], Monson and Seegmiller [5] and Cheah et al. [6] using laser Doppler velocimetry (LDV) concern the first type of U-bends. The velocity field in sharp corner bends was investigated by Liou et al. [7] by LDV, Son et al. [8] by two-dimensional particle image velocimetry (PIV) and Schabacker et al. [9] by stereoscopic PIV. All studies highlighted the presence of secondary flows driven by the imbalance between the centrifugal forces and the radial pressure gradient. For sufficiently high curvature (i.e. low radius ratio), separation occurs along the inner wall in the second half of the bend.

U-bend geometries make an excellent test case for turbulence models, as the effects of the streamlines curvature and the associated secondary flows are typically challenging to reproduce in numerical simulations. The broad trends can be captured by two-equation eddy-viscosity models, provided that the boundary layer is resolved without recurring to wall functions, as discussed by Iacovides and Launder [10]. Recently, Lucci et al. [11] and Schueler et al. [12], using eddy-viscosity models, found overall agreement with experiments. However two-equation models cannot predict the effect of streamline curvature on the turbulence structure due to their inability to account for turbulence anisotropy. Calculations based on second moment closure were shown to provide more accurate predictions, e.g. in the two-pass channels studied by Bonhof et al. [13] and Chen et al [14]. Nevertheless, due to their reduced computational cost, two-equation models are still the standard tool employed in the design process in industrial applications.

The high pressure penalty imposed by the U-bend has fostered the interest towards strategies to improve the aerodynamic performance, especially in sharp turn configurations. Metzger et al. [15] varied the width of the passages, the corner radius and the clearance height, finding that the latter parameter had a substantial impact, with the pressure drop increasing for smaller clearances. The influence of the divider wall thickness was explored by Liou and Chen [16]. They found that a thicker wall reduces the turbulence level and shortens the reattachment length of the recirculating cell in the downstream half of the bend. Bonhof et al. [17] showed that inserting turning vanes alleviates the pressure loss. Schueler et al. [18], while confirming that properly designed vanes significantly reduce the pressure drop, also underlined that poorly designed vanes can actually deteriorate the aerodynamic performance.

All the above-mentioned studies concerned with the minimization of the U-bend pressure drop follow a classic trial-and-error approach: several configurations are generated varying a number of geometrical parameters, performances are compared and global trends are evaluated. However, given the large number of parameters, this type of design process remains extremely time-consuming. Moreover, as many of the parameters are strongly coupled, the relations between them and their effects are difficult to assess. In order to ease and speed up the process, so called optimization methods can be applied. Most of these techniques exploit natural principles to obtain effective solutions, while minimizing the intervention of the human designer. A recent example is the study of Zehner et al. [19], who optimized the divider wall of a sharp turn U-bend. They used the ice-formation technique to generate a starting profile of minimum energy dissipation, and further improved the performance applying an evolutionary algorithm. Namgoong et al. [20] used Design of Experiment and surrogate design space model for similar purposes.

This paper continues the work on the design of a smooth U-bend of radius ratio 0.76, optimized for minimal pressure loss as presented in [21] and validated experimentally in [22]. Within the present work an extension towards heat transfer is made in the design optimization process, leading to two conflicting requirements, namely to minimize the pressure losses in the bend and at the same time to maximize the heat transfer. This is translated into a multi-objective design optimization problem.

Both conflicting objectives are achieved using an incompressible Navier-Stokes solver in conjunction with a metamodel-assisted multi-objective Differential Evaluation (DE) algorithm. The profiles of the internal and external side of the bend are parameterized using piece-wise Bezier curves and are subject of optimization. The pressure loss and heat transfer is computed by the Navier-Stokes solver, which is based on a two-equation turbulence model. The multi-objective DE algorithm searches for trade-off solutions between both conflicting objectives and results in a Pareto front, which allows the designer still to make a choice after the optimization process finishes.

NOMENCLATURE

Latin

C	user defined constant
DE	Differential Evolution
DOE	Design of Experiments
E	expected value
EA	Evolutionary Algorithm
F	user defined constant
FVM	Finite Volume Method
MSE	Mean Square Error
P	pressure
RSM	response surface model
a,b,c	design vectors
f	objective function
r	random variable
t	generation index
v	velocity
x	design vector

Greek

ε	dissipation rate of turbulent kinetic energy
ρ	density

OPTIMIZATION METHOD

The optimization method used is the result of more than one decade of research conducted at the von Karman Institute [21, 22, 23]. The system (Fig. 1) makes use of a Differential Evolution algorithm (DE), a metamodel, a database, and a Finite Volume Method (FVM) CFD solver. The basic idea behind this method is a two-level optimization. A first one uses a rapid but less accurate analysis method (the metamodel) to evaluate the large number of geometries generated by the DE. The optimum geometry, according to the metamodel predictions, is then analyzed by the more accurate but much more computationally expensive FVM calculations to verify the accuracy of the metamodel predictions. The outcome of such an optimization cycle is added to the database. It is expected that, after a new training on the extended database, the metamodel will be more accurate as it is based on more information and the outcome of the next DE optimization will be closer to the real one. The optimization cycle is repeated until the Navier-Stokes results confirm the accuracy of the metamodel predictions.

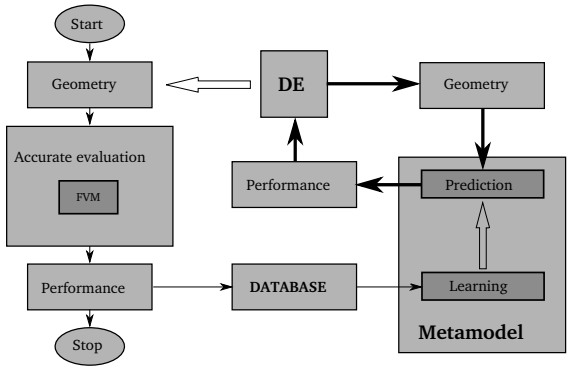

Figure 1 Flow chart of the optimization algorithm.

Geometry

The U-bend under investigation is typical of internal cooling channels. The baseline geometry is show in Fig. 2. It consists of a circular U-bend with radius ratio of 0.76, a hydraulic diameter of 0.075 meter and an aspect ratio of 1. The Reynolds number is 40.000 and the Mach number of 0.05 allows using an incompressible assumption. The shape of the inner and outer curve is allowed to be changed but needs to remain inside the bounding box shown in the figure, which restricts the height and width of possible changes to account for structural limits. The distance between both cooling channels is not subject to optimization, as well as the hydraulic diameter.

Parameterization

The parameterization of both inner and outer curve is shown in Figs. 3 and 4. Both curves are composed of 4 Bezier curves. The 180 degree turn is split into 2 Bezier curves, while the curves connecting the inlet with the U-bend and the U-bend with the outlet are defined by single Bezier curves. Each Bezier curve is a third order curve defined by a polynomial of 4 control points. By changing the coordinates of these control points the shape of the curve will change. This allows controlling the shape of the U-bend by several well-chosen parameters.

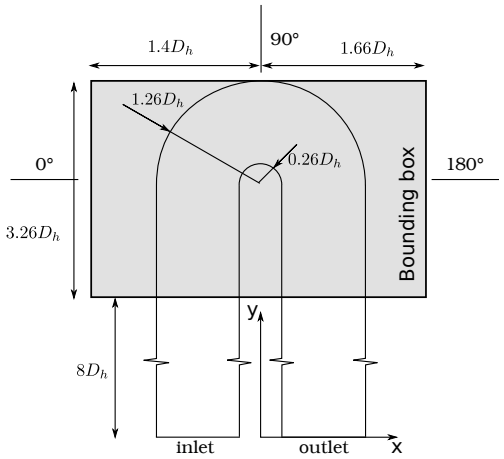

Figure 2: Baseline geometry, definition of area in which the shape is allowed to change.

The 4 curves defining the outer curve of the U-bend are parameterized by a total of 12 degrees of freedom, shown by arrows in Fig. 3. Several control points are only allowed to change in one direction while their other direction is controlled by the position of a neighboring control point to guarantee G1 continuity. The 3rd control point of curve 2 is for instance only allowed to move in the horizontal direction while it follows the vertical movement of the 4th control point of that curve such that the curve remains horizontal in its endpoint. In the last control point of the first curve, 3 degrees of freedom are specified: the horizontal and vertical movement of the control point and the curvature in that location. The curvature defines the vertical distance between the last and before last control point of curve 1 and the distance between the first and second control point of curve 2. The use of a curvature parameter guarantees a G2 continuity at the junction between curve 1 and 2, which is considered necessary after some preliminary studies. However, at the symmetrical control point between curve 3 and 4, no curvature specification is needed. As a result, the before last control point of curve 3 and the second control point of curve 4 have a vertical degree of freedom.

The parameterization of the inner curve is similar to the one of the outer curve, although for some control points the definition is based on the position of the control points of the outer curve. The last control point of the first curve is for instance positioned in the horizontal direction by a distance D1 from the same control point of the outer curve. The parameters D2 and D3 define their respective control points in a similar way. This parameterization introduces parameters closely related to the flow physics, compared to a parameterization where the x- or y-coordinates would have been specified. This

allows a more linear and direct relation between parameters and objective, as the acceleration of the flow is the result of one single parameter and not the difference between two parameters defined at inner and outer curve. This makes the optimization problem well-posed.

The number of parameters defining the inner curve is 14. The total number of parameters for the entire U-bend is 26, which is a trade-off between a large freedom in shape and the need for an effective optimization. For each parameter suitable ranges are defined.

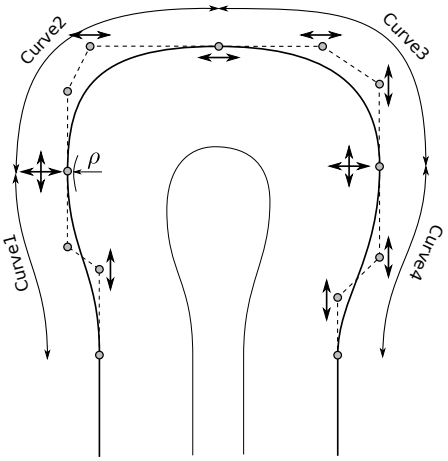

Figure 3: Parameterization of the outer curve.

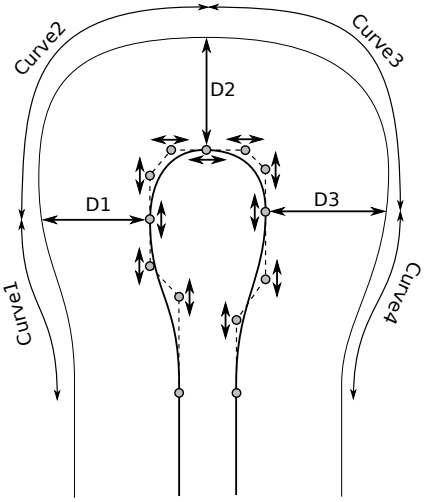

Figure 4: Parameterization of the inner curve.

Grid generation

A structured grid with 342x50x50 (855,000) cells has been used. The mesh is generated by an automated Gambit [26] script and allows for local refinement in regions of high curvature. In Fig. 5 a typical 2D view of the grid is shown. The boundary layer has been refined in accordance to the necessity of the Launder-Sharma low-Reynolds $k-\varepsilon$ turbulence model. The maximum y+ value does not exceed 2.2.

The k-ε model "is arguably the simplest complete turbulence model" (Pope [27]), is implemented in most commercial software and is one of the most broadly employed at industrial level. Its performance is reasonably satisfactory in shear flows with small effects of streamwise pressure gradients and streamline curvatures, but far from these assumptions, it can fail badly. However it has been selected for the present application due to its large diffusion: given that the proposed methodology is apt for industrial problems, it was the intention of the authors to demonstrate its potential in conditions that are representative of real-life design practice. Moreover, in the previous work [21-22], satisfactory global performance predictions compared to measurements were obtained with this model.

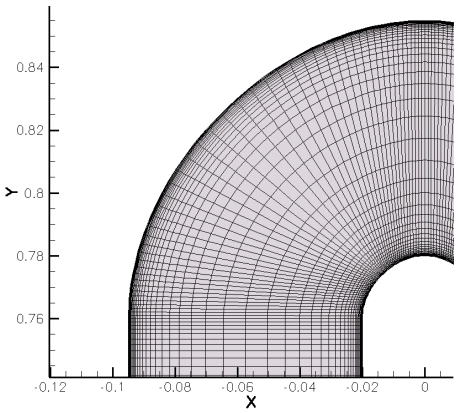

Figure 5: Zoom on the grid in the U-bend.

Performance evaluation

The simpleFoam solver from OpenFoam [28] is used to evaluate the incompressible Navier-Stokes equations. It has been extended to enable the calculation of thermal transport. It is a RANS solver for steady-state incompressible turbulent flow. The temperature field and its initial and boundary conditions are created similar to the velocity and pressure fields. The temperature equation is solved after the SIMPLE loop in each iteration.

At the inlet a fully developed velocity profile is imposed, together with values of k and ε for the turbulence model. Both are computed based on a turbulence intensity of 5% measured in the lab. At the outlet the static pressure is imposed. The wall temperature is set to be constant at 343.15K. The inlet temperature is initially kept uniform at 293.15K until a fully developed temperature profile is obtained. A convergence criteria of 5.10^{-6} for the residuals is imposed. The computations are run in parallel on 5 cores, requiring an average of 2 hours per calculation.

The U-bend optimization is driven by the minimization of the pressure drop introduced by the U-bend and the

maximization of the heat transfer. The objective functions are formulated as:

$$\min f_1(\vec{x}) = \frac{P_{total}^{inlet} - P_{total}^{outlet}}{1/2 \cdot \rho \cdot v_{ref}^2} \quad (1)$$

$$\max f_2(\vec{x}) = \frac{Q}{Q_{ref}} \quad (2)$$

where $\vec{x}$ is the design vector containing the 26 parameters describing the geometry (see Figs. 2 and 3) and Q is the total heat transferred to the fluid. The total pressure is computed as the mass flow averaged quantity at the inlet respectively outlet of the domain, positioned 8 hydraulic diameters away from the U-bend. The total pressure loss is non dimensionalized by the inlet dynamic pressure, with a reference velocity of 8.40 m/s.

$$P_{total} = \frac{\int_S p_{total} \cdot \rho v \cdot dS}{\int_S \rho v \cdot dS} \quad (3)$$

The heat transfer Q is computed from the overall enthalpy rise, and equals the integral of the heat flux on the wetted walls A (including the inlet leg and outlet leg). It is non dimensionalized by the heat transfer of the reference circular U-bend, which is 298 W.

$$Q = \dot{m} \cdot c_p \cdot \Delta T = \iint_A q_{wall} \cdot dA \quad (4)$$

Multi-objective Differential Evolution

Evolutionary Algorithms (EA) have been developed in the late sixties by J. Holland [29] and I. Rechenberg [30]. They are based on Darwinian evolution, whereby populations of individuals evolve over a search space and adapt to the environment by the use of different mechanisms such as mutation, crossover and selection. Individuals with a higher fitness have more chance to survive and/or get reproduced.

When applied to design optimization problems, EAs have certain advantages above gradient based methods. They do not require the objective function to be continuous and are noise tolerant. In the presence of local minima, they are capable of finding global optima and avoid to get trapped in a local minimum. Moreover, these methods can efficiently use distributed and parallel computing resources since multiple evaluations can be performed independently. The evaluation itself does not necessarily need to be made parallel. Disadvantages of EAs are mainly related to the large number of function evaluations needed.

Differential Evolution (DE) is a relatively new evolutionary method developed by Price and Storn [31]. It is easily programmable, does only require a few user defined parameters and performs well for a wide variety of these parameters. A determination of optimal user defined parameters is very often unnecessary.

Differential evolution, like all EAs, is population based and requires at each iteration the evaluation of an entire population of designs. The nomenclature resembles the one of evolutionary processes. A design vector $\vec{x}$ is called an individual; the collection of individuals at one given iteration is called a population, and the evolution of a population happens within generations, i.e. the children of the current population form the next generation.

The purpose of the algorithm is to find the individual $\vec{x}$ which minimizes an objective function $f(x)$. To describe one version of the single-objective DE [30], the *t*-th generation containing T individuals is considered. Each individual $\vec{x}_t$ contains *n* parameters.

$$\vec{x}_t = (x_1, x_2, ..., x_n) \quad (5)$$

To evolve the parameter vector $\vec{x}_t$, three other parameter vectors $\vec{a}_t$, $\vec{b}_t$ and $\vec{c}_t$ are randomly picked such that $\vec{a}_t \neq \vec{b}_t \neq \vec{c}_t \neq \vec{x}_t$. A trial vector $\vec{y}_t$ is defined as

$$y_i = a_i + F \cdot (b_i - c_i) \quad , \qquad i = 1..n \quad (6)$$

where F is a user defined constant ($F \in]0,2[$) which controls the amplification of the differential variation $(b_i - c_i)$. This procedure is usually called the mutation. The candidate vector $\vec{z}_t$ is obtained by a recombination operator involving the vectors $\vec{x}_t$ and $\vec{y}_t$, and is defined as

$$z_i = \begin{cases} y_i & if \quad r_i \leq C \\ x_i & if \quad r_i > C \end{cases} \quad i = 1..n \quad (7)$$

where r_i is a uniformly distributed random variable ($0 \leq r_i < 1$) and C is a user defined constant ($C \in]0,1[$). This procedure is usually called the crossover, in analogy with Genetic Algorithms (GA).

The final step in the evolution of $\vec{x}_t$ involves the selection process and, for the minimization of the objective function $f(x_t)$, is given by

$$x_{t+1} = \begin{cases} z_t & if \quad f(z_t) \leq f(x_t) \\ x_t & if \quad f(z_t) > f(x_t) \end{cases} \quad (8)$$

The selection process involves a simple replacement of the original parameter vector with the candidate vector if the objective function decreases by such an action.

Repeating the previous defined operations on each individual of the t-th generation will lead to a next generation (the t+1 th) with individuals with at least the same performance of the parent population due to Eqn. (8). Generation after generation individuals generated by random mutation will replace their ancestors when they perform better. The closer the population approaches the optimum of the objective function f, the smaller the mutations (Eqn. (6)) will become, which results in a more local search towards the optimum.

Many strategies exist to extend DE to multi-objective problems. Most of the algorithms are based on similar techniques used in GAs [32,33]. Rai [34] introduces a selection of parents based on the distance in objective space. The idea is that in the final stages of the optimization, the differential variation (b_i-c_i) should result from individuals close to the selected individual x_t. As such, the method behaves similar to a single-objective DE, where in the final stages the differential variations reduce in magnitude, as all individuals locate near the optimum. In the methods of Abbas et al. [32] and Madavan [33], the distance in parameter space between the different individuals of the Pareto front can be very large, even in the final stages of the evolution. This will result in large changes of the proposed individual z, which is an unwanted feature. By favoring the individuals close to x_t in the selection of the individuals a_t, b_t and c_t, this is avoided. The later method is implemented in the present work.

Metamodel assisted Differential Evolution

The major drawback of evolutionary algorithms such as DE is the total number of evaluations of the objective function needed. In general, more than a thousand evaluations are commonly needed, and depending on the complexity of the optimization problem (both number of parameters and complexity of the objective function), this number can drastically increase.

One way of reducing the unrealistic number of evaluations can be obtained by replacing the expensive evaluations (involving FVM) by a computationally cheaper method. This could be achieved by using a metamodel, which is a sort of interpolation tool using the already analyzed individuals by the FVM analysis.

The metamodel performs the same task as the high fidelity FVM analysis, but at a very low computational cost. However, it is less accurate, especially for an evaluation far away from the already analyzed points in the design space.

The implementation of the metamodel into the optimization system depends on how the system deals with the inaccuracy of the model. The technique used in the present work uses the metamodel as an evaluation tool during the entire evolutionary process [35]. After several generations the evolution is stopped and the best individual is analyzed by the expensive analysis tool. This technique is referred to as the "offline trained metamodel". The difference between the predicted value of the metamodel and the high fidelity tool is a direct measure for the accuracy of the metamodel. Usually at the start this difference is rather large. The newly evaluated individual is added to the database used for the interpolation and the metamodel will be more accurate in the region where previously the evolutionary algorithm was predicting a minimum. This feedback is the most essential part of the algorithm as it makes the system self-learning. It mimics the human designer which learns from his mistakes on previous designs.

Within the present study, a Kriging metamodel has been used and replaces the CFD evaluation during the search for both objectives with the DE algorithm. After the optimization phase, all individuals are located on the Pareto front, for which the objectives have been computed with the Kriging metamodel. A validation of these shapes by a CFD evaluation is necessary, however, not all Pareto optimal shapes need to be evaluated as this would not increase the metamodels knowledge effectively, as many entries will be added to the database which are close to each other in design space. Instead, only 5 candidate solutions are extracted from the Pareto front and analyzed by the CFD tool. These individuals are chosen with a distance metric, such that they are equally spread over the Pareto front.

Kriging

Kriging was initially developed by geologists to estimate mineral concentrations based only on scarce data available at some places of an area [36]; about the same time it was also introduced in the field of statistics to include the correlations that exist between residuals of a linear estimator [37]. The theory behind interpolation and extrapolation by kriging was developed by the mathematician G. Matheron based on the Master's thesis of D. G. Krige [38] on the use of the statistical techniques to predict the gold grades at the Witwatersrand reef complex in South Africa.

There are many texts in geostatistics [39, 40] and in spatial statistics [41-43] that provide many details on the development and use of kriging models in their respective disciplines. Recently, kriging became of interest to approximate deterministic computer models due to its capability of not only predicting a value, but also to give the uncertainty of the prediction. Several authors can be found that use kriging methods for accelerating an optimization process [44- 49].

Kriging belongs to the family of linear least squares algorithms, such as polynomial response surface models (RSM), however it is reproducing the observed data exactly. The mathematical form of a kriging model has two parts as shown in Eqn. (9). The first part is a linear regression with an arbitrary number k of regression functions g_j, that tries to catch the main trend of the response. An RSM model can be used for this purpose, however many authors (e.g. [45,49]) use a constant value for this part and rely on the second part of the model to pull the response surface through the observed data [46].

$$\tilde{f}(\vec{x}) = \sum_{j=1}^{k} \beta_j g_j(\vec{x}) + Z(\vec{x}) \qquad (9)$$

The second part, Z(x), is a model of a Gaussian and stationary random process with zero mean. An assumption is made on the mathematical form of the covariance of Z(x), which is usually a Gaussian function [49]. The parameters β_j and the function Z(x) are determined such that $\tilde{f}(\vec{x})$ is the best linear unbiased predictor. A linear estimator means that $\tilde{f}(\vec{x})$ can be written as a linear combination of the observation samples:

$$\tilde{f}(\vec{x}) = \sum_{i=1}^{N} \omega_i(\vec{x}) f_i(\vec{x}) \tag{10}$$

The unbiasedness constraint means that the mean error of the approximation is zero:

$$E\left[f(\vec{x}) - \tilde{f}(\vec{x})\right] = 0 \tag{11}$$

The best linear unbiased predictor is considered the predictor with minimal mean square error (MSE) of the predictions,

$$MSE = E\left[\left(\tilde{f}(\vec{x}) - f(\vec{x})\right)^2\right] \tag{12}$$

One big advantage of kriging above other metamodels is its ability to not only predict the value of the objective function, but also the uncertainty on the prediction (see Fig. 6). The details of constructing kriging models have been thoroughly described in [50, 51, 45, 52, 53, 43].

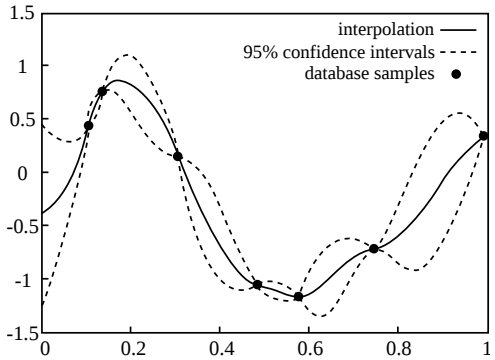

Figure 6: Prediction of mean value and confidence intervals by kriging.

The database

The accuracy of the metamodel predictions strongly depends on the information contained in the database. The Design Of Experiments (DOE) method is used to create the initial database. This maximizes the amount of information contained in it for a limited number of geometries [54].

Each design variable can take two values fixed at 25% and 75% of the maximum design range. A 2^{k-p} factorial design is used. k is the total number of design parameters (26) while p defines the number of lower order parameter combinations that are not analyzed. p is chosen such that in total 2^6=64 samples are generated for the initial database. An additional sample with all parameters at 50% of their range is added, resulting in a total of 65 initial geometries to be analyzed.

RESULTS

In Fig. 7 the result of the optimization is summarized. It shows the total pressure drop versus the heat extracted for all 220 analyzed geometries. The baseline geometry consisting of the circular U-bend is indicated by a square, while the 65 samples generated for the initial database by DOE are represented by black dots. It is already apparent from the DOE that all geometries perform better with respect to the total pressure drop objective, and most samples also perform better in the heat objective compared to the baseline.

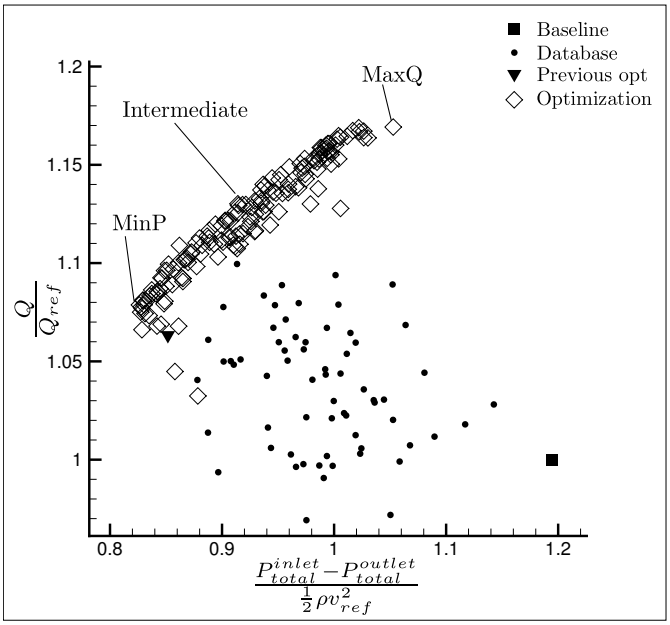

Figure 7. Results of the optimization plotted in objective space.

The samples generated during a total of 32 generations of the optimization phase are represented by diamonds. All of them are generated in the region of interest, i.e. with high heat transfer and low pressure drop. A clear Pareto front is formed, for which one cannot improve one objective without worsening the other. This clearly indicates that pressure loss and heat transfer are conflicting requirements, i.e. a physical mechanism is responsible to increase one and at the same time decrease the other.

Three candidate solutions are identified as "MinP" which has the lowest total pressure drop, "MaxQ" which has the highest heat transfer, and "Intermediate", which is in between both extremes. The performance of all three Pareto optimal geometries is summarized in Table 1. Finally, the optimal solution found during the single objective optimization, as presented in [21-22], is plotted as a gradient symbol. Although this optimization was not targeting any heat transfer objective, it improved the heat transfer compared to the baseline, as was also found during experimental validation [22]. The best candidate found within the current optimization ("MinP") outperforms the previously found optimum, this is thought to be because of a more accurate metamodel as it is trained with a larger diversity of samples, not only limited by the search for one single objective as was performed in [21].

Table 1. Performance of baseline and 3 Pareto optimal shapes.

	Total pressure drop [Pa]	Heat transfer [W]
Original	51.61	297.99
"MinP"	35.71	321.45
"Intermediate"	39.51	336.79
"MaxQ"	45.50	348.43

In Fig. 8 the shapes corresponding to the three identified candidates are shown. The geometry with lowest pressure drop ("MinP") resembles very closely the shape of the single-objective optimum [21], not shown here. The increase in heat transfer by going to "MaxQ" is obtained by increasing the curvature in the external wall in the first 90 degrees and by increasing the internal wall width. Both actions increase the pressure loss and transform the smooth configuration into one that resembles closer and closer a sharp u-bend configuration. Similar to what was found by Liou and Chen [16], a thicker divider wall is beneficial for the losses.

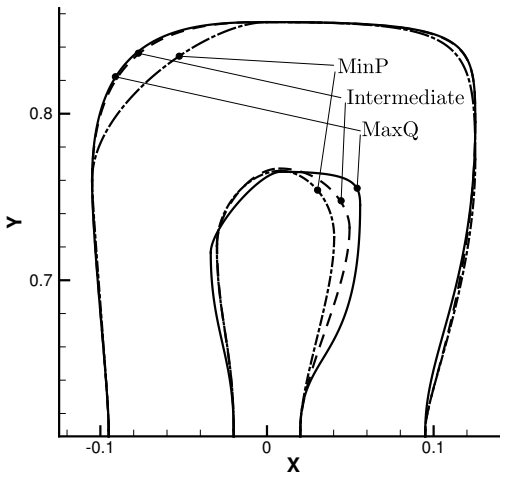

Figure 8. Comparison of the different optimized shapes.

Figures 9 and 10 show the streamlines and velocity at mid-span location for the configuration with lowest losses ("MinP") and the one with highest heat transfer ("MaxQ") respectively. In the "MinP" configuration, the thickness of the divider wall is gradually increased towards the 180 degrees turn, without accelerating the flow as the external wall moves along. The flow is then turned 180 degrees using a larger radius of curvature as compared to the circular arc baseline geometry, resulting in a smaller pressure gradient perpendicular to the fluid motion and hence with a smaller acceleration of the flow on the inner curve. At the same time, the channel widens. Finally, in the last part of the u-bend, the channel width is converging and hence accelerating the flow. It is in this region of the circular arc baseline geometry that a strong adverse pressure gradient exists, leading to separation of the flow. Within the optimized configuration, the separation is suppressed completely by a reduction of the adverse pressure gradient due to the larger radius of curvature and the diverging-converging shape of the channel.

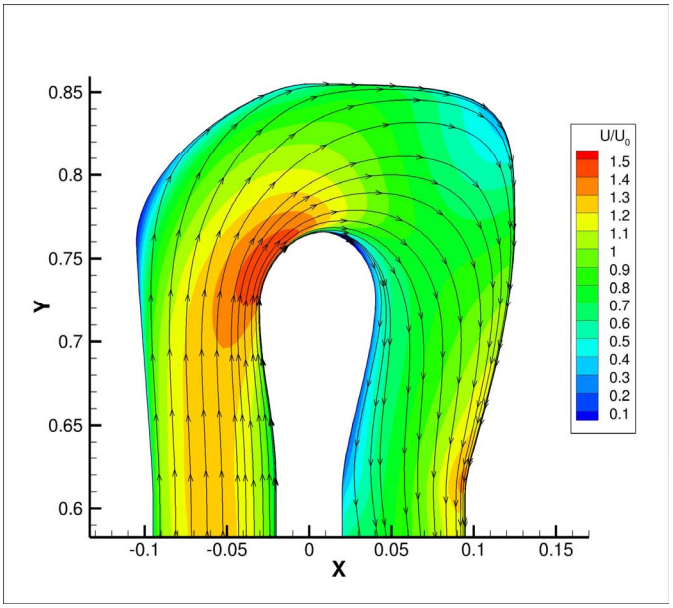

Figure 9. Mid-span streamlines in the optimal geometry for minimal pressure drop, "MinP".

On the other hand, for the "MaxQ" configuration of Fig. 10, the divider wall is increased substantially in thickness while the curvature is less smooth, with abrupt changes at 3 locations. This causes the flow to accelerate and decelerate several times on the inner curve, opposed to the smooth acceleration and deceleration of the "MinP" configuration. Nevertheless, with the limiting assumptions of the *k-ε* model, the flow remains attached under these unfavorable conditions. The diverging-converging feature of the channel, as found in the "MinP" configuration, remains. The external wall has a higher curvature in the first part of the bend. Combined with the higher curvature of the internal wall, a higher secondary flow motion is created,

with a larger normal velocity component towards the external wall in the middle of the 180 degree turn. This will result in a much higher heat transfer coefficient, as it resembles a jet impinging on a wall. In a similar way a higher normal velocity component is obtained near the exit of the turn, also increasing the local heat transfer.

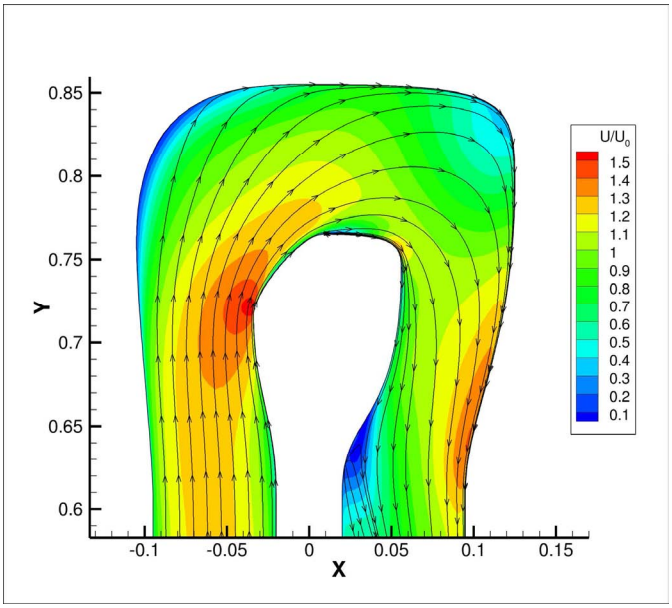

Figure 10. Mid-span streamlines in the optimal geometry for maximum heat transfer, "MaxQ".

Comparison between Figs. 11 and 12 confirms the higher heat transfer of "MaxQ". Both figures show the local Nusselt number on the walls of the channel. An increase in convective heat transfer at 90 degrees and 180 degrees on the external wall is found in both configurations, which is due to an impingement effect. However, this effect is more pronounced on the "MaxQ" configuration, due to a stronger secondary flow motion, as shown in detail in Fig. 13.

The total heat extracted is larger in the "MaxQ" configuration because of the higher heat transfer as demonstrated by the Nusselt number comparison, but as well due to a larger total wetted surface. The internal wall, although also enlarged in area, does however not play a significant role. The "MaxQ" configuration shows a larger non-uniformity in the Nusselt number and hence might increase the induced thermal stresses in the surrounding material, possibly reducing the benefits of the larger heat extraction.

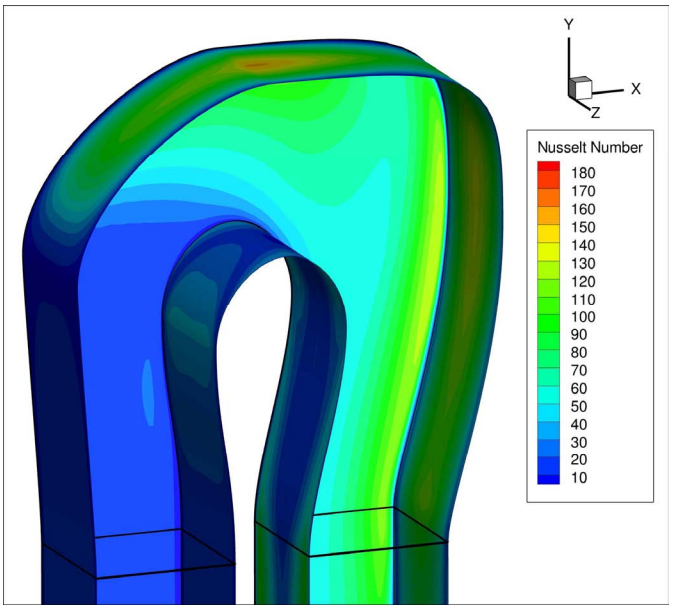

Figure 11. Nusselt number distribution in the optimal geometry for minimal pressure drop, "MinP".

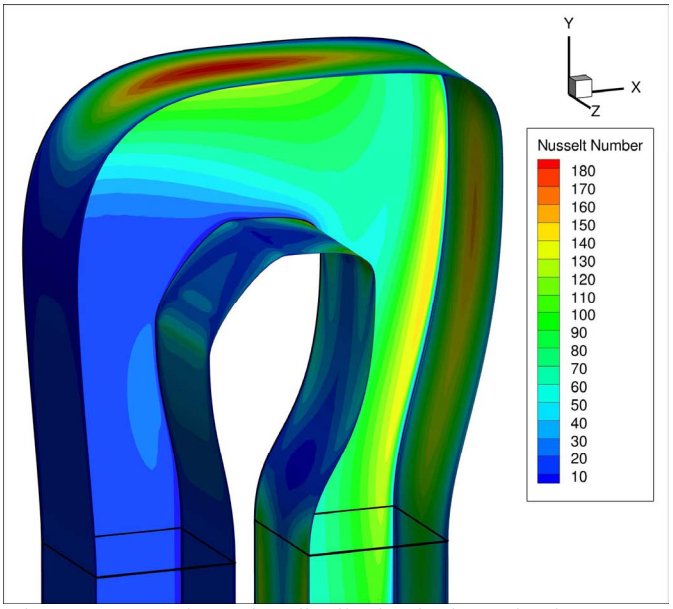

Figure 12. Nusselt number distribution in the optimal geometry for maximum heat transfer, "MaxQ".

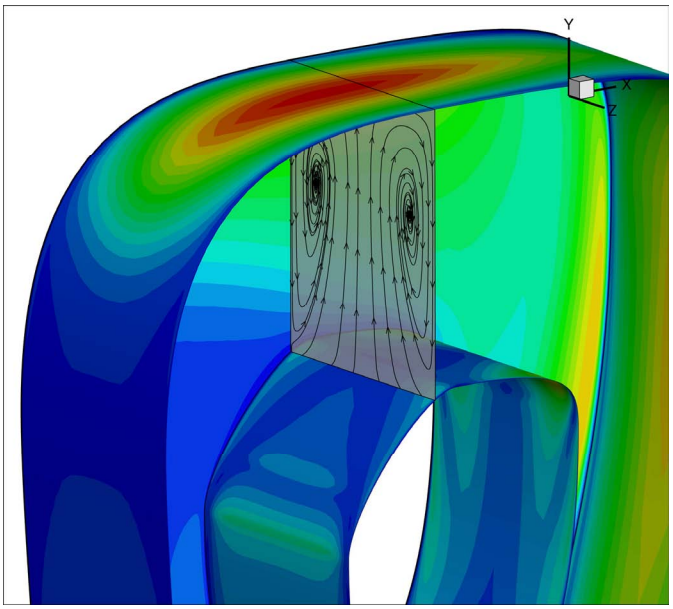

Figure 13. Secondary flow motion in the 90 degree plane of "MaxQ".

CONCLUSIONS

A multi-objective optimization method has been applied to the design of a u-bend. It uses an automated design procedure involving a Navier-Stokes solver, a metamodel, a database and an evolutionary algorithm.

Heat transfer and pressure loss objectives have been considered simultaneously in this work, leading to a Pareto front expressing the trade-off between both. Geometries with low pressure loss tend to have a smooth curvature change, and successfully suppress separation by increasing the radius of the turn and by carefully decelerating first and then accelerating the mean flow. As a consequence, less secondary flow motion is present and reduces the heat transfer potential. Geometries with high heat transfer on the other hand contain rapid changes of curvature and resemble close to sharp u-bends. Heat transfer is enhanced due to the impingement of the flow near the external wall, however increasing the losses.

It has been shows that the applied optimization method is cost-effective and allows to obtain significant improvements within a limited timeframe. It results in several trade-off results from which an experienced designer can select one that fits his requirements.

REFERENCES

[1] Han J.-C., Dutta S., Ekkad S., 2000. Gas Turbine Heat Transfer and Cooling Technology. Taylor and Francis, New York.

[2] Weigand B., Semmler K., von Wolfersdorf J., 2006. Heat Transfer Technology for Internal Passages of Air-Cooled Blades for Heavy-Duty Gas Turbines. Annals of the New York Academy of Sciences 934, pp. 179-193

[3] Humphrey J. A. C , Whitelaw J. H., Yee G., 1981. Turbulent Flow in a Square Duct with Strong Curvature. J of Fluid Mech 103, pp. 443-463.

[4] Chang S. M., Humphrey J. A. C, Modavi A., 1983. Turbulent Flow in a Strongly Curved U-Bend and Downstream Tangent of Square Cross-Sections. Physico-Chemical Hydrodynamics 4, pp. 243-269.

[5] Monson D.J., Seegmiller H. L., 1992. An Experimental Investigation of Subsonic Flow in a Two Dimensional U-Duct. NASA report TM-103931.

[6] Cheah S.C., Iacovides H., Jackson D.C., Ji H.H., Launder B.E., 1996. LDA Investigation of the Flow Development Through Rotating U-ducts. J. Turbomachinery 118, 590-596.

[7] Liou T.-M., Chen C.-C., 1999. LDV Study of Developing Flow Through a Smooth Duct With a 180 deg Straight-Corner Turn. J Turbomach, 121(1), pp. 167-174

[8] Son S.Y., Kihm K.D., Han J.-C., 2002. PIV Flow Measurements for Heat Transfer Characterization in Two-Pass Square Channels With Smooth and 90° Ribbed Walls. Int J Heat and Mass Trans 45, pp. 4809-4822

[9] Schabacker J., Boelcs A., Johnson B. V., 1998. PIV Investigation of the Flow Characteristics in an Internal Coolant Passage with Two Ducts Connected by a Sharp 180deg Bend. ASME paper 98-GT-544.

[10] Iacovides H., Launder B. E., 1996. Computational Fluid Dynamics Applied to Internal Gas-Turbine Blade Cooling: A Review. Int J Heat and Fluid Flow 16, pp. 454-470.

[11] Lucci J. M., Amano R. S., Guntur K., 2007. Turbulent Flow and Heat Transfer in Variable Geometry U-Bend Blade Cooling Passage, ASME paper GT2007-27120.

[12] Schüler M., Neumann S. O., Weigand B., 2010. Numerical Investigations of Pressure Loss and Heat Transfer in a 180° Bend of a Ribbed Two-Pass Internal Cooling Channel with Engine-Similar Cross-Sections, J of Power and Energy 224, pp. 349-361

[13] Bonhoff B., Tomm U., Johnson B. V., 1996. Heat Transfer Predictions for U-Shaped Coolant Channels with Skewed Ribs and With Smooth Walls. ASME paper 96-TA-7.

[14] Chen H.-C., Jang Y.-J., Han J.-C., 2003. Computation of Heat Transfer in Rotating Two-Pass Square Channels by a Second-Moment Closure Model. Int J Heat Mass Transfer 43, pp. 1603-1616.

[15] Metzger D. E., Plevich C. W., Fan C. S., 1984. Pressure Loss Through Sharp 180◦ Turns in Smooth Rectangular Channels. J of Engineering for Gas Turbine and Power 106, pp. 677-681.

[16] Liou T.-M., Tzeng Y.-Y, Chen, C.-C., 1999. Fluid Flow in a 180◦ Sharp Turning Duct With Different Divider Thicknesses. J Turbomach 121, pp. 569-576.

[17] Bonhoff B., Leusch J., Johnson B. V., 1999. Predictions of Flow and Heat Transfer in Sharp 180-deg Turns of Gas Turbine Coolant Channels with and without Turning Vanes, 33rd National Heat Transfer Conference, Albuquerque, NM, USA.
[18] Schüler M., Zehnder F., Weigand B., von Wolfersdorf J., Neumann S.O., 2011. The Effect of Turning Vanes on Pressure Loss and Heat Transfer of a Ribbed Rectangular Two-Pass Internal Cooling Channel. J Turbomach 133, 021017 (10 pages).
[19] Zehner S., Steinbrück H., Neumann S. O., Weigand B., 2009. The Ice Formation Method: A Natural Approach to Optimize Turbomachinery Components. Int J of Design & Nature 3, pp.259–272
[20] Namgoong H., Son C., Ireland P., 2008. U-bend Shaped Turbine Blade Cooling Passage Optimization. AIAA paper ISSMO 2008-5926
[21] T. Verstraete, F. Coletti, J. Bulle, T. Vanderwielen, T. Arts. Optimization of a U-Bend for Minimal Pressure Loss in Internal Cooling Channels – Part I: Numerical Method. ASME Tubo Expo, Paper No. GT2011-46541, June 6-11, 2011, Vancouver, Canada
[22] F. Coletti, T. Verstraete, T. Vanderwielen, J. Bulle, T. Arts. Optimization of a U-Bend for Minimal Pressure Loss in Internal Cooling Channels – Part II: Experimental Validation. ASME Tubo Expo, Paper No. GT2011-46555, June 6-11, 2011, Vancouver, Canada
[23] Pierret, S., 1999, "Designing Turbomachinery Blades by Means of the Function Approximation Concept Based on Artificial Neural Network, Genetic Algorithm, and the Navier-Stokes Equations", Ph.D. Thesis, Faculté Polytechnique de Mons-Von Karman Institute for Fluid Dynamics.
[24] Pierret, S., and Van den Braembussche, R.A., 1999, "Turbomachinery Blade Design Using a Navier Stokes Solver and Artificial Neural Networks", ASME journal of turbomachinery, Vol. 121, pp.326-332.
[25] Verstraete, T., "Multidisciplinary Turbomachinery Component Optimization Considering Performance, Stress, and Internal Heat Transfer",Ph.D. Thesis, Universty of Ghent-Von Karman Institute.
[26] Gambit Academic Research, Release 2.4.6, URL http:// www.ansys.com
[27] Pope S. B., 2000. Turbulent Flows, Cambridge University Press.
[28] Open Foam, URL http://www.openfoam.com.
[29] Holland, J.H., 1975, "Adaption in Natural and Artificial Systems", University of Michigan Press.
[30] Rechenberg, I., 1973, "Evolutionsstrategie — Optimierung technischer Systeme nach Prinzipien der biologischen Evolution", Fommann-Holzboog, Stuttgart.
[31] Price, K., and Storn, N., 1997, "Differential Evolution", Dr. Dobb's Journal, pages 18–24, April.
[32] H. A. Abbas, R. Sarker, and C. Newton. PDE: A Pareto-Frontier Differential Evolution Approach for Multi-objective Optimization Problems. In Proceedings of the Congress on Evolutionary Computation, volume 2, pages 971-978, Piscataway, New Jersey, 2001.
[33] N. K. Madavan. Multiobjective Optimization Using a Pareto Differential Evolution Approach. In Proceedings of the Congress on Evolutionary Computation, volume 2, pages 1145-1150, Honolulu, Hawaii, 2002.
[34] M. Rai. Single and multiple objective optimization with differential evolution and neural networks. In VKI Lecture Series on Introduction to Optimization and Multidisciplinary Design in Aeronautics and Turbomachinery, Brussels, June 2008.
[35] Verstraete, T., 2010, "CADO: a Computer Aided Design and Optimization Tool for Turbomachinery Applications", Presented at 2nd Int. Conf. on Engineering Optimization, Lisbon, Portugal, September 6-9, 2010.
[36] Matheron, G., 1963, "Principles of Geostatistics", Economic Geology, 58:1246–1266.
[37] Goldberger, A.S., 1962, "Best Linear Unbiased Prediction in the Generalized Linear Regression Model", Journal of the American Statistical Association, 57(298):369–375.
[38] Krige, D.G., 1951, "A statistical approach to some mine valuations and allied problems at the Witwatersrand",. PhD thesis, University of Witwatersrand.
[39] Goovaerts, P., 1997, "Geostatistics for Natural Resources Evaluation", Oxford Univ. Press, New York.
[40] Journel, A.G., and Huijbregts, C.J., 1978, "Mining Geostatistics", Academic Press, New York.
[41] Cressie, N. A. C., 1991,"Statistics for Spatial Data", Wiley, New York.
[42] Ripley, B.D., 1981, "Spatial Statistics", Wiley, New York.
[43] Stein, M.L., 1999, "Interpolation of Spatial Data: Some theory of Kriging", Springer-Verlag, New York.
[44] S. E. Gano, S. S., and Renaud, J.E., 2005, "Hybrid Variable Fidelity Optimization by Using a Kriging-Based Scaling Function", AIAA Journal, 43(11):2422–2430.
[45] Jeong, S, Murayama, M, and Yamamoto, K., 2005, "Efficient Optimization Design Method Using Kriging Model", Journal of Aircraft, 42(2):413–420.
[46] Martin, J. D., and Simpson, T.W., 2005, "Use of Kriging Models to Approximate Deterministic Computer Models", AIAA Journal, 43(4):853–863.
[47] Martin, J. D., and T. W. Simpson, T.W., 2004, "A Monte Carlo Simulation of the Kriging Model", AIAA Paper No. 2004-4483.

[48] Simpson, T W., 1998, “Comparison of Response Surface and Kriging Models in the Multidisciplinary Design of an Aerospike Nozzle”, ICASE Report No.98-16.
[49] Simpson, T. W., Peplinski, J.,Koch, P. N., and Allen, J.K., 200, “Metamodels for Computer-Based Engineering Design: Survey and Recommendations”, Engineering with Computers, 17(2):129–150.
[50] Denison, D. G. T., Holmes, C. C., Mallick, B. K., and Smith, A. F. M., 2002, “Bayesian Methods for Nonlinear Classification and Regression”, Willey, New York.
[51] Guinta, A. A., and Watson, L. T.,1998, “A Comparison of Approximation Modeling Techniques: Polynomial Versus Interpolating Models”, AIAA Paper No. 98-4758.
[52] Jones, D. R., Schonlau, M., and Welch, W. J., 1998,”Efficient Global Optimization of Expensive Black-Box Functions”, Journal of Global Optimization, 13(4):455–492.
[53] Simpson, T. W., Mauery, M. T., Korte, J. J., and Mistree, F., 2001,” Kriging Metamodels for Global Approximation in Simulation-Based Multi-Disciplinary Design Optimization”, AIAA Journal, 39(12):2233–2241.
[54] Montgomery, D.C., 1997, “Design and Analysis of Experiments”, John Wiley and Sons, New York.